



# Studies on Multiferroic Behavior of Y-Mn Co-Doped $\text{Bi}_{0.9}\text{La}_{0.1}\text{FeO}_3$

P. Josely Jose<sup>1,4</sup> · Urjitsinh Rathod<sup>1</sup> · Chirag Savaliya<sup>1</sup> · Sadaf Jethva<sup>1</sup> · Akshay Panchasara<sup>2</sup> · Savan Katba<sup>3</sup> · Mukesh Keshvani<sup>4,5</sup> · Megha Vagadia<sup>6</sup> · Ashish Ravalia<sup>1</sup>

Received: 19 February 2022 / Accepted: 15 September 2022 / Published online: 11 October 2022  
© The Minerals, Metals & Materials Society 2022

## Abstract

To understand the multiferroic behavior of the Y and Mn co-doped  $\text{Bi}_{0.9}\text{La}_{0.1}\text{FeO}_3$  system, we have synthesized  $\text{Bi}_{0.9}\text{La}_{0.1}\text{FeO}_3$  with the co-doped composition of  $\text{Bi}_{(0.9-a)}\text{Y}_a\text{La}_{0.1}\text{Fe}_{(1-b)}\text{Mn}_b\text{O}_3$  ( $a=0.05, b=0.05, 0.10, 0.15, 0.20$ , and  $a=0.10, b=0.10$ ) using the solid-state reaction method. The role of Y and Mn co-doping on the structural, magnetic, ferroelectric, and dielectric properties were studied by various characterization techniques, such as x-ray diffraction, vibrating sample magnetometer (VSM), polarization–electric field (P–E) loop tracer, and dielectric measurements. X-ray diffraction studies show that a 5% doped sample is single phasic nature and crystallizes in rhombohedral (R3c) symmetry, whereas higher doped samples are dual-phase in nature with minor impurity  $\text{Bi}_2\text{Fe}_4\text{O}_9$  and crystallize in rhombohedral (R3c) and cubic (Pm-3 m) modulation in structural parameters with Y and Mn doping. The modulation in magnetic behavior with Y and Mn doping has been investigated and studied in the context of modification in the different interactions. P–E loop behavior is observed for lower Y (5%) and Mn (5, 10, 15%) doped samples, whereas a lossy/leaky loop is found for higher doped samples (Y-5, 10%, and Mn-20%). Lastly, the real and imaginary parts of dielectric permittivity indicate doping-induced increases in the values of  $\epsilon'$  and  $\epsilon''$ .

**Keywords** Multiferroics · bismuth ferrite (BFO) · magnetic properties · ferroelectric · dielectric

## Introduction

Perovskite materials having the general formula  $\text{ABO}_3$  are desirable because of their excellent physical properties, which can be used in a variety of technological applications. Multiferroics (MF) exhibit two or more “ferroic” orders that have been studied and have recently piqued the interest of

materials scientists due to their wide range of practical applications in data storage, multiple state memories, condensers, transducers, and so forth.<sup>1–3</sup> Out of the several MFs studied so far,  $\text{BiFeO}_3$  (BFO), is a well-known multiferroic compound due to its showing multiferroic properties at room temperature.

$\text{BiFeO}_3$  is widely studied due to the coupling between the ferroelectric and magnetic order at room temperature, which creates the possibility of room temperature multiferroic devices. It shows rhombohedral R3c symmetry, G-type antiferromagnetic Néel,  $T_N \sim 370^\circ\text{C}$ , and ferroelectric Curie up to  $T_C \sim 830^\circ\text{C}$ .<sup>4–7</sup> Consequently, the validity of BFO in devices is limited due to various factors such as oxygen vacancy, leakage currents, and so on. Despite certain advantageous properties, BFO has some inherent issues due to the spatially modulated spin structure, which prevents net magnetization and inhibits the observation of a significant linear magnetoelectric effect.<sup>8,9</sup> Pure BFO has severe leakage issues, making it practically unusable. The significant leakage current was due to the low concentration of  $\text{Fe}^{2+}$  ions and oxygen vacancies in perovskite materials.<sup>10</sup> To reduce this inherent problem (leakage current) and to enhance

✉ Ashish Ravalia  
ashishravalia@gmail.com

<sup>1</sup> Department of Nanoscience and Advanced Materials, Saurashtra University, Rajkot 360005, India

<sup>2</sup> Department of Electronics, Saurashtra University, Rajkot 360005, India

<sup>3</sup> Department of Physics, School of Science, RK University, Rajkot 360020, India

<sup>4</sup> Department of Physics, Marwadi University, Rajkot 360003, India

<sup>5</sup> Present Address: The Patidar Gin Science College, Bardoli 394601, India

<sup>6</sup> Indian Institute of Science Education and Research, Bhopal 462066, India

ferroelectric and ferromagnetic order parameters, studies on the effect of doping at either the Bi-site or Fe-site and/or optimizing synthesis parameters have been reported.<sup>11</sup> Based on various reports, doping at the A and B sites is quite effective in improving multiferroic properties. In the literature survey, many reports are available on the effects of doping on the Bi-site (La, Ca, Ba, Sr, Nd, Sm, Tb, Pb)<sup>12–16</sup> and Fe-site (Mn, Co, Cr, Ti, Ni).<sup>17–20</sup> Significant studies in recent years have shown that the multiferroic characteristics of BFO may be considerably tuned toward an ideal multiferroic material by using appropriate doping.<sup>21,22</sup> Several groups have attempted to enhance the ferroelectric polarization and remnant magnetization and decrease the leakage current of BFO by suitably doping with rare earth elements such as La<sup>3+</sup>, Nd<sup>3+</sup>, Gd<sup>3+</sup>, Sm<sup>3+</sup>, and so on.<sup>12</sup> It has been reported that substituting Bi<sup>3+</sup> with La<sup>3+</sup> having similar radii to Bi<sup>3+</sup> could reduce Bi volatilization and oxygen vacancy concentration in BFO, resulting in structural stability and the removal of the impurity phase.<sup>23</sup>

Enhancement in multiferroic behavior due to doping with Y has been reported by Zhong et al.<sup>24</sup> has reported that the impurity phase of bismuth ferrite disappears when Y doping concentration increases. Bellaki and Manivannan<sup>25</sup> have determined that 10% Y leads BFO to an orthorhombic-like symmetry transformation. However, doping with Mn has been investigated and shown to reduce leakage currents. Srinivas et al.<sup>26</sup> reported that increasing Mn in BFO shows a marginal change in structure and enhancement in magnetization. Another report on Mn doping in BFO shows the improvement of multiferroic properties.<sup>27,28</sup> However, co-doping is a far more efficient way to tailor the magnetoelectric properties of BFO. Several groups have attempted to enhance the electrical and magnetic properties of BFO by co-doping.<sup>29,30</sup> Thus, considering these studies, it will be helpful to comprehend the impact of La and Y doping at the Bi-site and Mn at the Fe-site in modifying the Fe valence state in BFO, which might lead to enhanced electrical and magnetic properties.<sup>31–33</sup>

In the present communication, we report the results of our studies on the influence of RE doping (La, Y) at the Bi-site (A-site) and Mn at the Fe-site (B-site) co-doping in the BiFeO<sub>3</sub> system, prepared by solid-state reaction (SSR). The main objective of this work is to understand the role of Y and Mn co-doping in the BLFO multiferroics by analyzing their structural, microstructural, dielectric, polarization–electric field (P–E) loop, and magnetic properties. Here, we have chosen Bi<sub>0.9</sub>La<sub>0.1</sub>FeO<sub>3</sub> due to its stable crystal structure compared with pure BiFeO<sub>3</sub>.<sup>4</sup>

## Experimental

Conventional solid-state reaction route, Y-Mn co-doped Bi<sub>0.9</sub>La<sub>0.1</sub>FeO<sub>3</sub> (BLFO) with the stoichiometric composition Bi<sub>(0.9-a)</sub>Y<sub>a</sub>La<sub>0.1</sub>Fe<sub>(1-b)</sub>Mn<sub>b</sub>O<sub>3</sub> (a = 0.05, 0.10, b = 0.05, 0.10, 0.15, 0.20) was used for synthesis, and hereafter referred to as YMn5, YMn10, YMn15, YMn20, and Y10Mn10. High purity powders of Bi<sub>2</sub>O<sub>3</sub>, La<sub>2</sub>O<sub>3</sub>, Y<sub>2</sub>O<sub>3</sub>, Mn<sub>2</sub>O<sub>3</sub>, and Fe<sub>2</sub>O<sub>3</sub> (99.99% purity Sigma-Aldrich) were weighed in stoichiometric proportions and mixed thoroughly in an agate mortar for 4–5 h until a homogeneous mixture was formed. Then, the mixtures were calcined at 600°C for 2 h. The calcined powders were again ground for 4–5 h and pressed into pellets having a diameter of ~ 10 mm and thickness of ~ 1 mm using the hydraulic press at a pressure of 4 × 10<sup>6</sup> Pa and were sintered at 810°C for 1 h. After sintering, the samples were characterized using the x-ray diffraction (XRD) technique with Cu-Kα (λ = 1.54 Å) to confirm the phase purity of the samples. Magnetic hysteresis (M–H) and temperature-dependent magnetic behavior were measured using a vibrating sample magnetometer (VSM). At room temperature, frequency-dependent dielectric measurements were carried out. Ferroelectric characterization was carried out using a Radiant P–E loop tracer.

## Results and Discussion

X-ray diffraction (XRD) patterns were analyzed to identify the crystal structural phase and purity of all the BLFO samples with different doping concentrations of Y and Mn. Figure 1 displays the atomic configuration of BLFO with YMn5 and YMn20 doped BLFO, respectively (generated through VESTA [Visualisation for Electronic Structural Analysis] software<sup>34</sup>). BFO has a rhombohedrally distorted perovskite-type structure of space group R3c. Figure 2a presents real-time (RT) XRD patterns of doped BLFO samples which show that, except for YMn5, the other BLFO (i.e., YMn10, YMn15, YMn20, and Y10Mn10) samples, which show minor impurity marked by\*, which is associated with Bi<sub>2</sub>Fe<sub>4</sub>O<sub>9</sub> phase formed due to the volatile nature of Bi and the high sintering temperature used during synthesis, which matches with the JCPDS file no. 01-072-1832.<sup>35</sup> Figure 2b shows the enlarged view of doubly split (104) and (110) XRD reflections (2θ from 30° to 35°) shifts towards a higher angle and merges into a single peak (110) with the increase in Y and Mn doping concentration, indicates the reduction in the unit cell due to the substitution of smaller ionic radii, Y (0.90 Å) with higher ionic radii, Bi (1.03 Å).<sup>31,32,35</sup> This clearly shows that a considerable crystal structural distortion has developed as a result of doping, which is caused by slight variations in the lattice parameters (Table I). As a

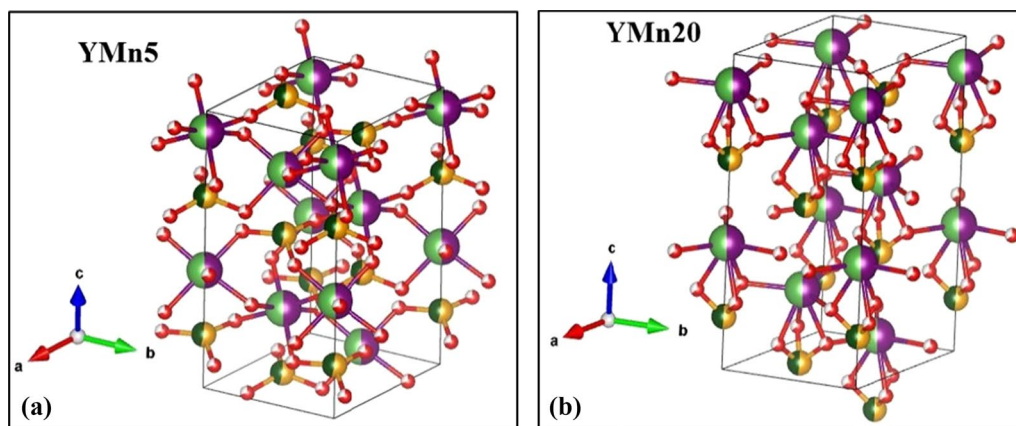


Fig. 1 (a) BLFO with YMn5 co-doped (b) YMn20 co-doped BLFO.

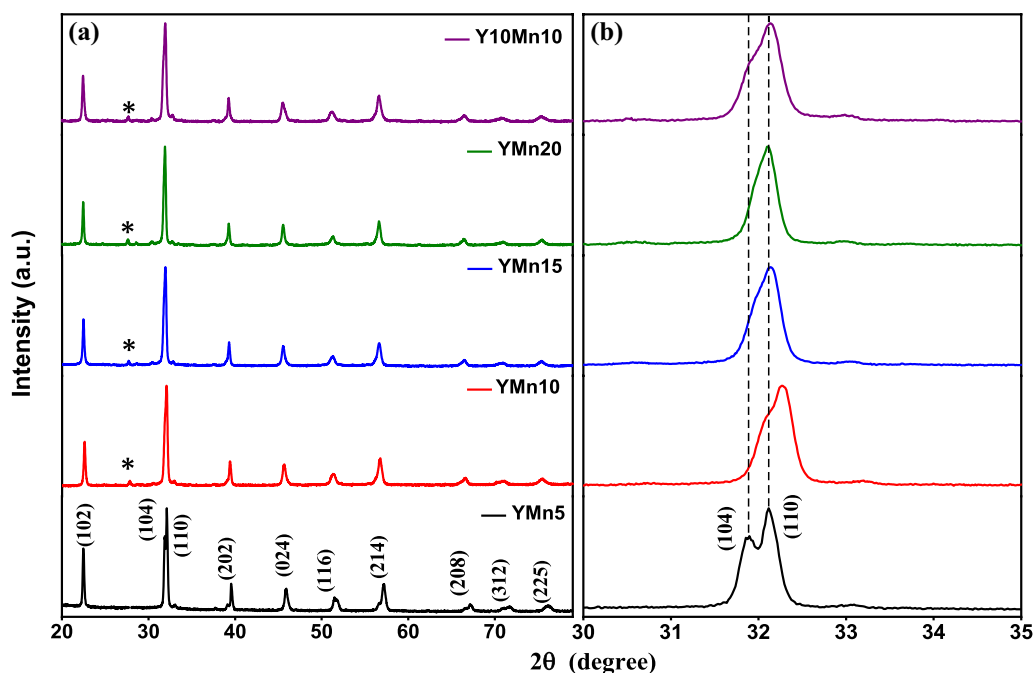


Fig. 2 (a) XRD patterns of YMn5, YMn10, YMn15, YMn20, and Y10Mn10. \*indicate peaks corresponding to  $\text{Bi}_2\text{Fe}_4\text{O}_9$  phase; (b) Enlarged view of the (104) and (110) peaks.

result, it is reasonable to conclude that doping with suitable elements and regulating their concentration will alter the structure of BLFO effectively.

To further confirm the structural transition, all the XRD patterns were refined using Rietveld refinement via the Full-Prof program,<sup>36</sup> and the fitted patterns are shown in Fig. 3. It can be seen from the plots that the samples crystallize in two phases, namely, rhombohedral (R3c) and cubic (Pm-3 m) except YMn5. Values of the Rietveld refined parameters are listed in Table I. It is noted that the values of S (goodness of fit) indicate that the fitting of the observed data and

calculated values are in good agreement. With increasing in Y and Mn concentrations, the transition from R3c to R3c + Pm-3 m is expected since the  $\text{Mn}^{3+}$  cation weakly destabilizes R3c as compared with that of  $\text{Fe}^{3+}$ , whereas  $\text{Y}^{3+}$  strongly destabilizes the R3c phase. Using Rietveld refinement for composition (YMn10, YMn15, YMn20, and Y10Mn10), we estimated the percentage of each phase present in the presently studied samples (Fig. 3). The decrease in lattice parameters leads to under-stress of lattice parameters with the increase in Y and Mn doping concentration. Thus, increasing the Y and Mn doping content changes the

crystal symmetry from rhombohedral to cubic. Furthermore, the volume drops slightly as the doping fraction increases, indicating a composition-driven structural phase transition. The relations between structural parameters and other properties are discussed in detail with electrical and magnetic data analysis.

Field-emission scanning electron microscopy (FE-SEM) was employed to study the surface morphology of the BLFO

**Table 1** Values of Rietveld refined XRD parameters of BFO doped Y-Mn samples

Parameters	R 3c	P m -3 m			
	YMn5	YMn10	YMn15	YMn20	Y10Mn10
a (Å)	5.5489	3.9370	3.9349	3.9345	3.9321
b (Å)	5.5489	3.9370	3.9349	3.9345	3.9321
c (Å)	13.7524	3.9370	3.9349	3.9345	3.9321
Volume (Å <sup>3</sup> )	366.71	61.02	60.93	60.91	60.80
R <sub>p</sub>	27.1	23.4	21.2	26.1	25.2
R <sub>wp</sub>	22.2	14.5	13.0	15.4	16.1
R <sub>exp</sub>	10.57	8.94	8.05	8.96	8.70
χ <sup>2</sup>	4.45	2.62	2.62	2.96	3.45
Gof	2.10	1.62	1.61	1.71	1.85
Avg. size (CS) (μm)	0.516	0.339	0.319	0.265	0.229

samples. Figure 4 represents the SEM images of the BLFO samples. Flat semi-oval and rectangular-shaped grains are observed in Y-Mn doped BLFO samples. The different Y-Mn content had a pronounced effect on the size, density, and homogeneity of the grains. With increasing Y-Mn content, the grain size of the doped samples tended to decrease, which was due to the inhibition of grain growth caused by Y-Mn co-doping. From the SEM analysis, it is observed that the grain size is about ~1 μm, and decreases slightly with the increase in Y-Mn doping. This is possible because upon higher doping secondary phases' precipitation releases stresses, and therefore SEM images show flat crystal faces, which is consistent with XRD results. In addition, the variation in morphology with doping content may be due to the Kirkendall effect, which leads to diffusion rates of constituting elements of the compounds.<sup>1,37</sup>

To understand the magnetic behavior of the presently studied system, M–T at 0.1 T and M–H at 5 K and 300 K measurements were carried out. Figure 5 shows the temperature dependence of the magnetic susceptibility measured under a magnetic field of 0.1 T in the range of 5–300 K in both zero-field-cooled (ZFC) and field-cooled (FC) protocols. The bifurcation of the ZFC–FC curve exhibits the coexistence of ferromagnetic and antiferromagnetic ordering of BFO nanoparticles, which is typically observed in the core–shell-like the structure of BFO nanoparticles.<sup>38</sup> In

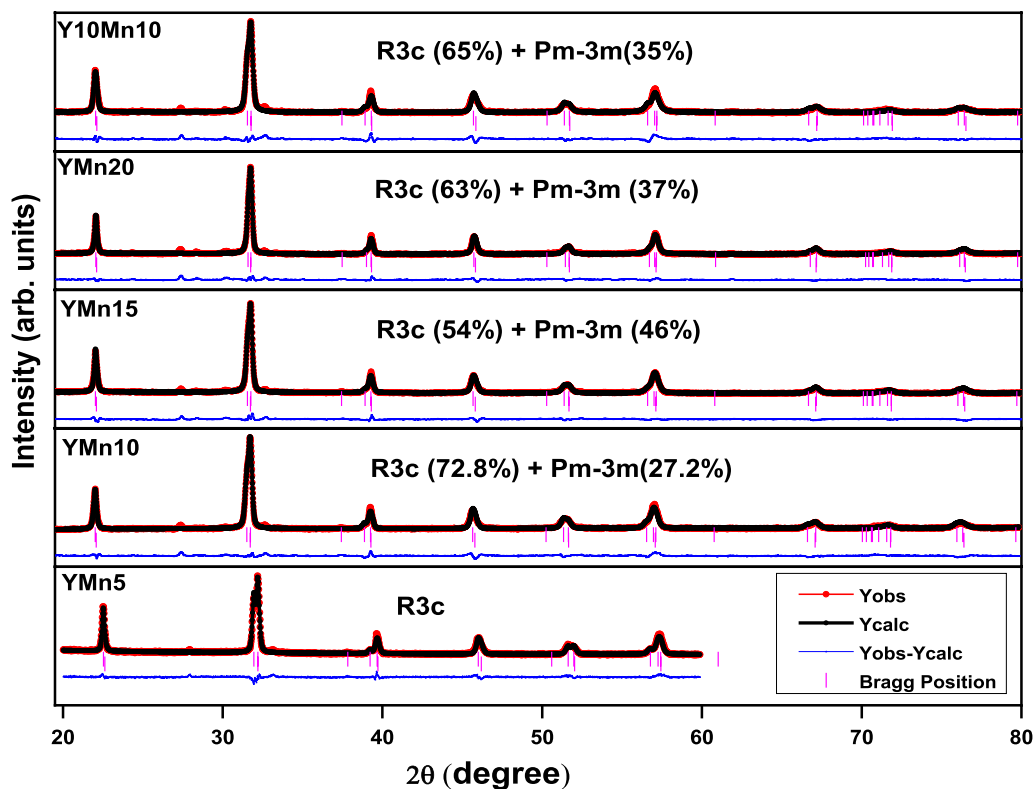


**Fig. 3** Rietveld Refinement XRD patterns of BLFO Y-Mn co-doped samples.

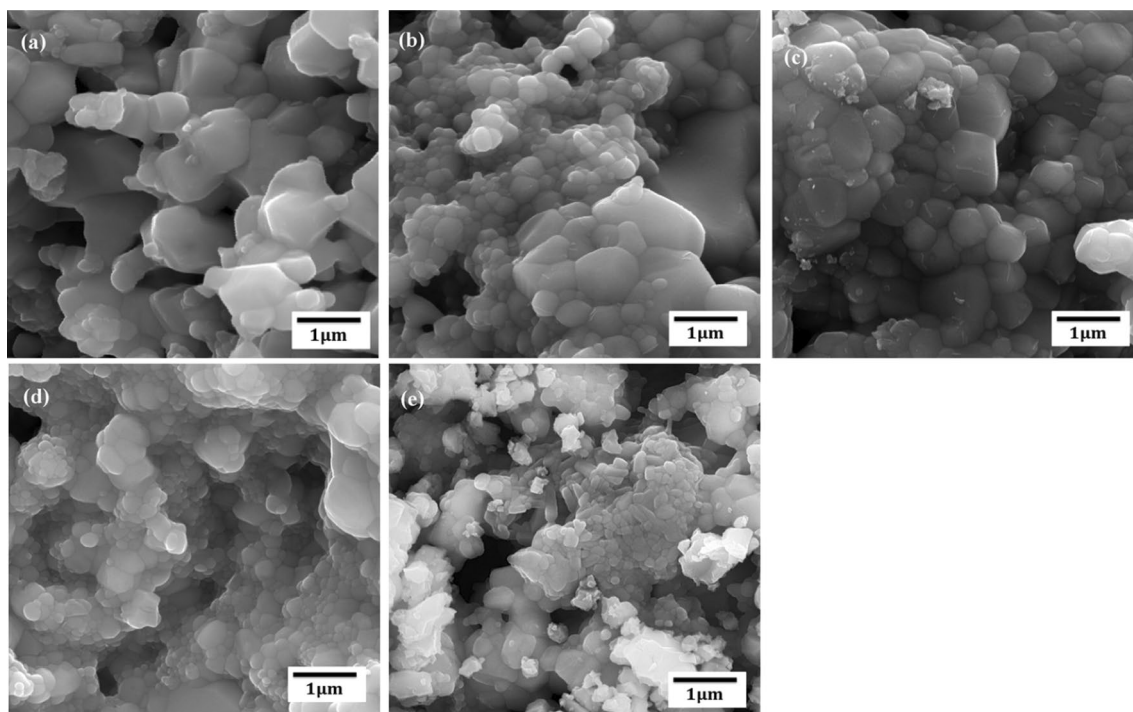


Fig. 4 SEM images of BLFO samples: (a) YMn5, (b) YMn10, (c)YMn15, (d) YMn20, (e) Y10Mn10.

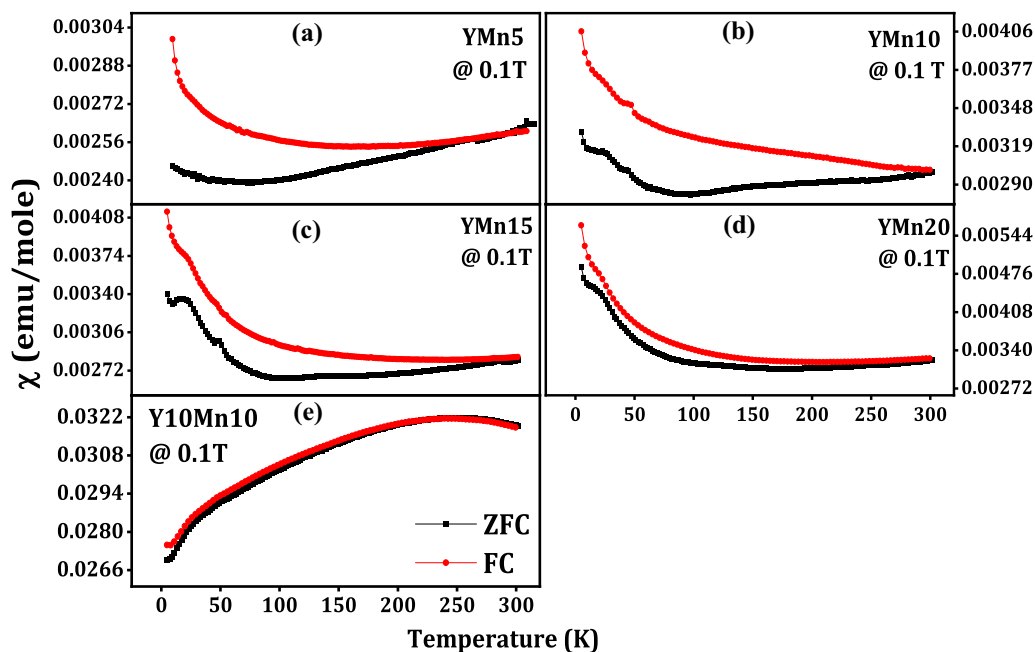


Fig. 5 ZFC and FC curves of co-doped BLFO samples (a) YMn5, (b) YMn10, (c) YMn15, (d) YMn20, and (e) Y10Mn10.

the present study, it is observed in Fig. 5a–d, that the ZFC and FC curves start to split below 300 K and a divergence between the curves increases as the temperature decrease, indicating the existence of the ferromagnetic property/weak ferromagnetic ordering,<sup>38,39</sup> whereas for Y10Mn10 (Fig. 5e)

they were found to overlap, in which magnetization increases with increasing temperature. The magnetic behavior of the proposed system can be understood in two different ways: (i) Fig. 5a–d in which YMn5, YMn10, YMn15, YMn20, and (ii) Fig. 5e Y10Mn10 BLFO system. In the first case,

(Fig. 5a–d),  $\chi$ -T curves show three different characteristics such as (i) decreased separation between FC and ZFC curves, (ii) Sharp increase the value of below 100 K and (iii) Observed low-temperature peak at  $\sim 9$  K with increased Mn substitution. The first two characteristics can be understood by La and Mn substitution-induced magnetization. This unusual magnetic behavior was similarly observed in the Mn-doped  $\text{Bi}_{1-x}\text{La}_x\text{FeO}_3$  system by Khomchenko et al.<sup>40</sup> The characteristics at the low-temperature peak are due to the effect of Y substitution, similarly observed in  $\text{YFeO}_3$ .<sup>41</sup> For YMn5 peak is not observed at  $\sim 9$  K due to the less effect of Y doping compared with La and Mn substitution-induced magnetization. In the second case (Fig. 5e),  $\chi$ -T curves show the unusual magnetic behavior due to higher substitution at the Bi-site, which induced distortion in the crystal structure. The unusual magnetic behavior of the Y10Mn10 system can be correlated with the modification in the crystal structure. The Rietveld refinement data clearly shows that  $\text{Fe}^{3+}\text{-O}^{2-}\text{-Mn}^{3+}$  angle increases max. at  $67.28^\circ$ , which can increase the  $\text{Fe}^{3+}\text{-O}^{2-}\text{-Mn}^{3+}$  interaction compared with  $\text{Fe}^{3+}\text{-O}^{2-}\text{-Fe}^{3+}$  resulting in a decrease in magnetization value with temperature. This behavior is quite similar to the Mn-doped  $\text{YFeO}_3$  system.<sup>42</sup> The U shape behavior of  $\chi$ -T (Fig. 5a–d) and peak or unusual behavior (Fig. 5e) is related to Mn doping in the BLFO system and the effect of Y magnetic ordering respectively. The overall value of magnetic susceptibility increases one order for Y10Mn10 due to higher doping of Y resulting in modifying the  $\text{Fe}^{3+}\text{-O}^{2-}\text{-Mn}^{3+}$  structure as discussed in the previous point.

To further investigate the magnetic characteristics of the sample, field-dependent magnetization measurements were

carried out. The magnetization as a function of applied magnetic field  $M(H)$  for all the co-doped BLFO samples was studied under applied magnetic fields at 5 K and 300 K, as shown in Fig. 6. The BLFO shows good magnetic hysteresis behavior due to the distorted antiferromagnetic spin cycloid of pure BFO and magnetically active  $\text{Y}^{3+}$  characteristics. Perfect magnetic hysteresis loops were observed at 5 K and 300 K for each composition and the saturation magnetization increased with an increase in  $\text{Mn}^{3+}$  content at RT. The higher saturation magnetization observed for YMn20 than other doped samples could be attributed to the higher lattice strain developed due to the beneficial effect of co-doping, which also agreed very well with the zero-field-cooled (ZFC) and field-cooled (FC) studies Fig. 5d. We noticed that the saturation magnetization increased at low temperatures compared with room temperature. The results show that the BLFO samples contain small remnant magnetization, which implies that they have a weak ferromagnetic behavior. The magnetization increases when Mn is the dopant due to the magnetic moment of Mn and the charge compensation effect. The enhanced magnetization owing to Mn and La co-doping was reported by Wu et al.<sup>43</sup> However, the observed magnetization value for our samples was small in comparison with those reported in the literature. This might be due to several factors such as synthesis technique, synthesis conditions, annealing conditions, and temperature.<sup>26</sup> With Fe valence state fluctuation and  $\text{Fe}^{2+}\text{-O-Fe}^{3+}$  super-exchange interaction induced by Y doping, Y influences Fe and the moment of Mn, which can enhance the magnetization.<sup>32</sup> However, it is notable that the coercive fields show slight variation with the substitution of  $\text{Y}^{3+}$ , and this behavior might be due to the distortion and shrinking of the BFO crystal cells.<sup>44</sup>

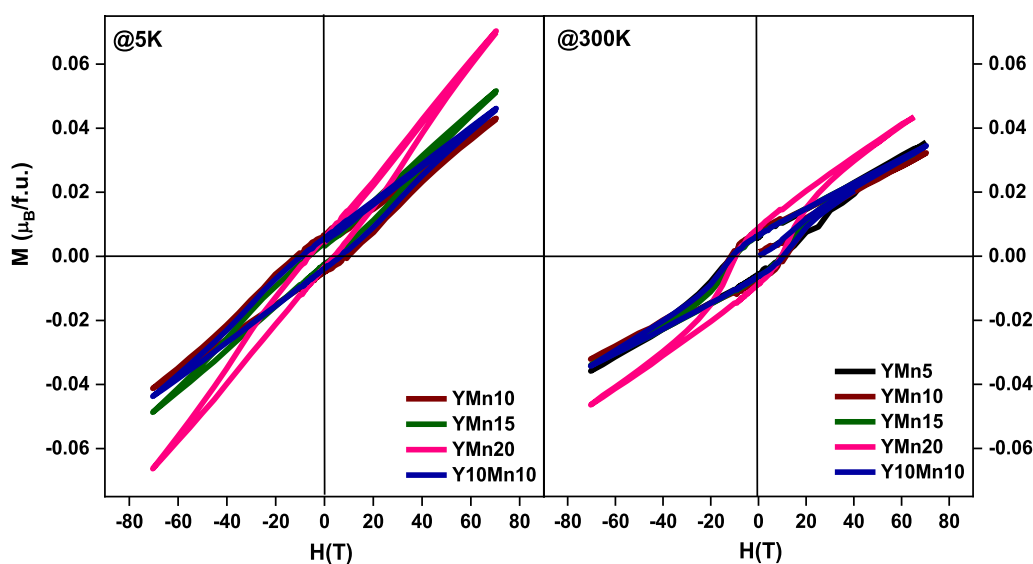


Fig. 6 M–H hysteresis loop of co-doped BLFO YMn5, YMn10, YMn15, YMn20, and Y10Mn10 at 5 K and 300 K.

All calculated parameters of M–H curves are summarized in Table II. As a result, the magnetic characteristics of the samples are greatly influenced by the doping concentration.

Figure 7 shows polarization–electric field (P–E) loops of Y and Mn co-doped BLFO at room temperature. Various drive fields were applied due to different breakdown fields exhibited. In an applied electric field of 250 kV/cm, non-saturated hysteresis P–E loops were observed. Ideally, measuring the steady P–E curves of the BLFO at room temperature in a high electric field area is challenging due to the breakdown caused by the large leakage current. This improvement in ferroelectric behavior in co-doped samples might be due to reduced charge defects such as oxygen vacancies.<sup>2</sup> The incorporation of yttrium ions in the bismuth site helps to reduce oxygen vacancies and the bismuth volatilization,<sup>32</sup> while the amount of the Mn doped in BLFO, a saturated P–E hysteresis loop could not be obtained due to the release of free charge carriers. It is observed that YMn5, YMn10, and YMn15

show the non-saturated hysteresis loop, but YMn20 and Y10Mn10 exhibit leaky behavior due to high Y and Mn doping. This behavior can be understood by the effect of doping. The increase in doping level of Mn increases oxygen vacancies and hence lossy/leaky behavior for the YMn20 sample. The formation of oxygen vacancies is indirectly calculated from the atomic ratio of Bi/Fe, which is ~0.98, ~0.97, ~0.96 for YMn5, YMn10, YMn15, and ~0.93, ~0.85 for YMn20, Y10Mn10, respectively (calculated from the EDX data). The EDX spectrum is given in the supplementary material. The EDX spectral analysis is given in Fig. S1 (see supplementary Figure S1) and it shows the presence and composition of the constituent element.

Figure 8 shows the frequency-dependent variation of the real ( $\epsilon'$ ) and imaginary ( $\epsilon''$ ) parts of the dielectric permittivity of the Y-Mn co-doped BLFO system at room temperature. Real ( $\epsilon'$ ) and imaginary ( $\epsilon''$ ) parts of the dielectric permittivity were calculated using the following equation.

$$\epsilon' = -\frac{d}{\omega\epsilon_0A} \left( \frac{Z''}{Z'^2 + Z''^2} \right) \text{ and } \epsilon'' = -\frac{d}{\omega\epsilon_0A} \left( \frac{Z'}{Z'^2 + Z''^2} \right)$$

where  $d$  = thickness of the sample,  $\omega$  = frequency,  $\epsilon_0$  = dielectric permittivity,  $A$  = area of the sample.  $Z'$  = real part of the impedance,  $Z''$  = imaginary part of impedance. It has been observed, that the values of real and imaginary dielectric permittivity ( $\epsilon'$ ,  $\epsilon''$ ) increase with Y and Mn doping content, while ( $\epsilon'$ ,  $\epsilon''$ ) decreases with increasing frequency. A high ( $\epsilon'$ ,  $\epsilon''$ ) value in the doped samples implies a smaller charge defect in the samples.<sup>45</sup> Usually, the dipolar, electronic, ionic, and interfacial polarization contribute to the real and

**Table II** Calculated values of  $M_r$  and  $H_c$  for the BLFO samples

Sample	Coercive field, $H_c$ (T) $10^3$		Remanent magnetization, $M_r$ (magnetization ( $\mu_B$ /f.u.))	
	5 K	300 K	5 K	300 K
YMn5	–	10.056	–	0.0058
YMn10	10.102	10.101	0.0053	0.0073
YMn15	10.103	10.040	0.0032	0.0063
YMn20	10.103	10.030	0.0042	0.0086
Y10Mn10	10.090	10.098	0.0063	0.0047

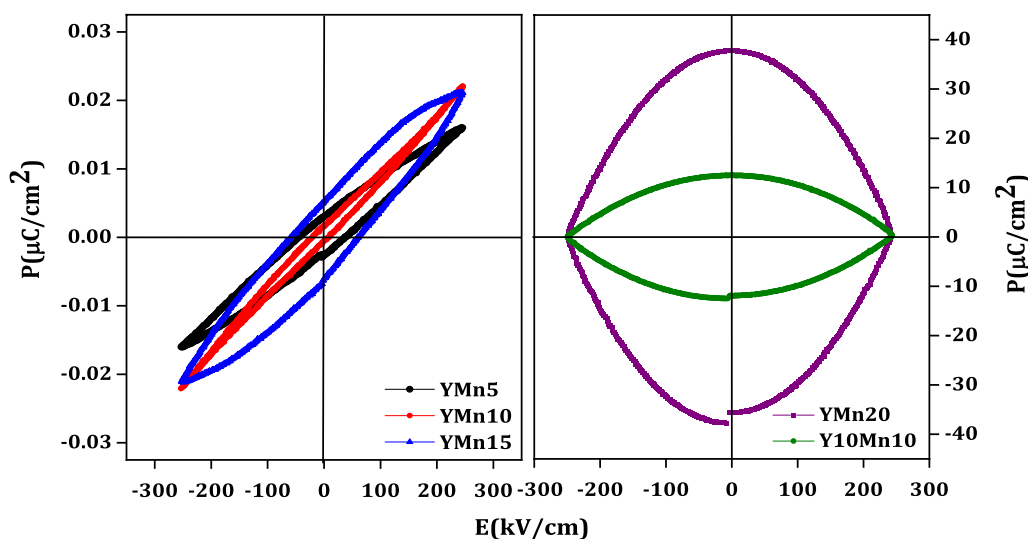


**Fig. 7** P–E hysteresis loop of Y-Mn co-doped BLFO samples.

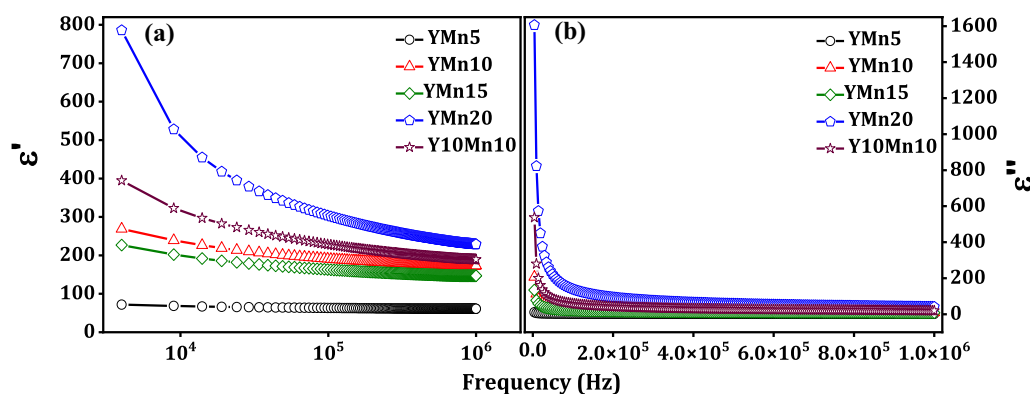


**Fig. 8** Variation of the (a) real part and (b) imaginary part of dielectric permittivity with frequency for Y-Mn co-doped BLFO.

imaginary dielectric permittivity of any material. Dipolar polarization contributes in the sub-infrared frequency range ( $10^3$ – $10^6$  Hz).<sup>46</sup> At low frequencies, dipolar and interfacial polarization is responsible for dielectric behavior, whereas atomic and electronic polarizations are effective at higher frequencies. In the present case, a decrease in the real and imaginary part of dielectric permittivity with an increase in frequency has been explained based on dipolar phenomena, which occur owing to the presence of defects and the doping of various elements in the BLFO system.

## Conclusion

We have successfully synthesized the Y-Mn co-doped  $\text{Bi}_{0.9}\text{La}_{0.1}\text{FeO}_3$  ( $a = 0.05$ ,  $b = 0.05$ ,  $0.10$ ,  $0.15$ ,  $0.20$ ) using conventional solid-state reaction technique. The Rietveld refinement XRD pattern indicates a single-phase rhombohedrally distorted (R3c) for YMn5, while the other samples crystallize in dual-phase, rhombohedral, and cubic (R3c + Pm-3 m) along with modulation in the crystal structure. The Y-Mn co doping significantly improves the dielectric, magnetic and ferroelectric properties of  $\text{Bi}_{0.9}\text{La}_{0.1}\text{FeO}_3$ . Temperature-dependent magnetic susceptibility measurements show different interactions of magnetic ions with the low-temperature ordering of Y, suggesting the sensitivity in magnetic behavior with Y and Mn substitution in BLFO. M–H measurements confirm the weak ferromagnetic behavior. Similar magnetic behavior, doping-induced change in dielectric behavior, and P–E loop have been investigated. The decrease in the dielectric constant with an increase in frequency may be due to the presence of defects which arise due to Y and Mn doping in the BLFO system. The increase in the unsaturated P–E hysteresis loop with Mn substitution up to 5–15% while higher doping of Y and Mn shows leaky behavior due to structural change. From the above studies,

it is confirmed that the multiferroic property of the BLFO system modifies with Y and Mn substitution.

**Supplementary Information** The online version contains supplementary material available at <https://doi.org/10.1007/s11664-022-09972-2>.

**Acknowledgments** The authors acknowledge Prof. D.G. Kuberkar, Saurashtra University, Rajkot for his guidance and motivation. The authors are thankful to the Department of Physics, Saurashtra University, Rajkot for providing the XRD and P–E loop facility. The authors thank Prof. A. K. Nigam, TIFR, for magnetization measurements. M.V. acknowledges DST, India for the INSPIRE faculty award (DST/INSPIRE/04/2017/003059). ABR is thankful to IUAC New Delhi for UFR-65319 and UGC-DAE, CSR, Indore for CSR-IC-ISUM-64/ CRS-347/2020-21/949 Project funding.

**Conflict of interest** We wish to confirm that there are no known conflicts of interest associated with this publication and there has been no significant financial support or personal relationships that could have appeared to affect the work reported in this paper. We confirm that the manuscript has been read and approved by all named authors and that there are no other persons who satisfied the criteria for authorship but are not listed. We further confirm that the authorship order listed in the manuscript has been approved by all of us.

## References

1. W. Eerenstein, N.D. Mathur, and J.F. Scott, Multiferroic and magnetoelectric materials. *Nature* 442, 759–765 (2006). <https://doi.org/10.1038/nature05023>.
2. J. Dho, X. Qi, H. Kim, J.L. MacManus-Driscoll, and M.G. Blamire, Large Electric Polarization and Exchange Bias in Multiferroic  $\text{BiFeO}_3$ . *Adv. Mater.* 18, 1445–1448 (2002). <https://doi.org/10.1002/adma.200502622>.
3. N.A. Hill and A. Filippetti, Why are There Any Magnetic Ferroelectrics? *J. Magn. Magn. Mater.* 242–245, 976–979 (2002). [https://doi.org/10.1016/S0304-8853\(01\)01078-2](https://doi.org/10.1016/S0304-8853(01)01078-2).
4. U. Nuraini and S. Suasmoro, Crystal Structure and Phase Transformation of  $\text{BiFeO}_3$  Multiferroics on the Temperature Variation. *J. Phys: Conf. Ser.* 817, 012059 (2017). <https://doi.org/10.1088/1742-6596/817/1/012059>.
5. A.J. Jacobson and B.E.F. Fender, A Neutron Diffraction Study of the Nuclear and Magnetic Structure of  $\text{BiFeO}_3$ . *J. Phys. C: Solid State Phys.* 11, 1031–1040 (1978).



- State Phys.* 8, 844–850 (1975). <https://doi.org/10.1088/0022-3719/8/6/015>.
6. W. Prellier, M.P. Singh, and P. Murugavel, The Single-Phase Multiferroic Oxides: From Bulk to Thin Film. *J. Phys.: Condens. Matter* 17, R803–R832 (2005). <https://doi.org/10.1088/0953-8984/17/30/R01>.
  7. J. Silva, A. Reyes, H. Esparza, H. Camacho, and L. Fuentes, BiFeO<sub>3</sub>: A Review on Synthesis, Doping and Crystal Structure. *Integr. Ferroelectr.* 126, 47–59 (2011). <https://doi.org/10.1080/10584587.2011.574986>.
  8. J. Schiemer, R. Withers, L. Noren, L. Yun, L. Bourgeois, and G. Stewart, Detailed Phase Analysis and Crystal Structure Investigation of a Bi<sub>1-x</sub>Ca<sub>x</sub>FeO<sub>3-x/2</sub> Perovskite-Related Solid Solution Phase and Selected Property Measurements Thereof. *Chem Mater.* 21, 4223–4232 (2009). <https://doi.org/10.1021/cm901757h>.
  9. D. Varshney, A. Kumar, and K. Verma, Effect of A Site and B Site Doping on Structural, Thermal and Dielectric Properties of BiFeO<sub>3</sub> Ceramics. *J. Alloys Compd* 509, 8421–8426 (2011). <https://doi.org/10.1016/j.jallcom.2011.05.106>.
  10. G.L. Yuan, K.Z. Baba-Kishi, J.M. Liu, S.W. Or, Y.P. Wang, and Z.G. Liu, Multiferroic Properties of Single-Phase Bi<sub>0.85</sub>La<sub>0.15</sub>FeO<sub>3</sub> Lead-Free Ceramics. *J. Am. Ceram. Soc.* 89, 3136–3139 (2006). <https://doi.org/10.1111/j.1551-2916.2006.01186.x>.
  11. H. Wu, Y.B. Lin, J.J. Gong, F. Zhang, M. Zeng, M.H. Qin, Z. Zhang, Q. Ru, Z.W. Liu, X.S. Gao, and J.M. Liu, Significant Enhancements of Dielectric and Magnetic Properties in Bi(Fe<sub>1-x</sub>Mg<sub>x</sub>)O<sub>3-x/2</sub> Induced by Oxygen Vacancies. *J. Phys. D: Appl. Phys.* 46, 145001 (2013). <https://doi.org/10.1088/0022-3727/46/14/145001>.
  12. S.T. Zhang, Y. Zhang, M.H. Lu, C.L. Du, Y.F. Chen, Z.G. Liu, Y.Y. Zhu, N.B. Ming, and X.Q. Pan, Substitution-Induced Phase Transition and Enhanced Multiferroic Properties of Bi<sub>1-x</sub>La<sub>x</sub>FeO<sub>3</sub> ceramics. *Appl. Phys. Lett.* 88, 162901 (2006). <https://doi.org/10.1063/1.2195927>.
  13. N. Jeon, D. Rout, I.W. Kim, and S.J.L. Kang, Enhanced Multiferroic Properties of Single-Phase BiFeO<sub>3</sub> Bulk Ceramics by Ho Doping. *Appl. Phys. Lett.* 98, 072901 (2011). <https://doi.org/10.1063/1.3552682>.
  14. P. Uniyal and K.L. Yadav, Room Temperature Multiferroic Properties of Eu Doped BiFeO<sub>3</sub>. *J. Appl. Phys.* 105, 07D914 (2009). <https://doi.org/10.1063/1.3072087>.
  15. G.L. Yuan, S.W. Or, J.M. Liu, and J.M. Liu, Structural Transformation and Ferroelectromagnetic Behavior in Single-Phase Bi<sub>1-x</sub>NdxFeO<sub>3</sub> Multiferroic Ceramics. *Appl. Phys. Lett.* 89, 052905 (2006). <https://doi.org/10.1063/1.2266992>.
  16. Z. Yan, K.F. Wang, J.F. Qu, Y. Wang, Z.T. Song, and S.L. Feng, Processing and Properties of Yb-Doped BiFeO<sub>3</sub> Ceramics. *Appl. Phys. Lett.* 91, 082906 (2007). <https://doi.org/10.1063/1.2775034>.
  17. A. Ravalia, M. Vagadia, P.S. Solanki, S. Gautam, K.H. Chae, K. Asokan, N.A. Shah, and D.G. Kuberkar, Role of Defects in BiFeO<sub>3</sub> Multiferroic Films and Their Local Electronic Structure by X-Ray Absorption Spectroscopy. *J. Appl. Phys.* 116, 153701 (2014). <https://doi.org/10.1063/1.4898196>.
  18. A. Ablat, E. Muhemmed, C. Si, J. Wang, H. Qian, R. Wu, N. Zhang, R. Wu, and K. Ibrahim, Electronic Structure of BiFe<sub>1-x</sub>Mn<sub>x</sub>O<sub>3</sub> Thin Films Investigated by X-Ray Absorption Spectroscopy. *J. Nanomater.* (2012). <https://doi.org/10.1155/2012/123438>.
  19. H. Liu, Z. Liu, and K. Yao, Improved Electric Properties in BiFeO<sub>3</sub> Films by the Doping of Ti. *J. Sol-Gel Sci Technol* 41, 123–128 (2007). <https://doi.org/10.1007/s10971-006-0514-x>.
  20. X. Qi, J. Dho, R. Tomov, M.G. Blamire, and J.L. MacManus-Driscoll, Greatly Reduced Leakage Current and Conduction Mechanism in aliovalent-Ion-Doped BiFeO<sub>3</sub>. *Appl. Phys. Lett.* 86, 062903 (2005). <https://doi.org/10.1063/1.1862336>.
  21. A. Mukherjee, M. Banerjee, S. Basu, P.M.G. Nambissan, and M. Pal, Gadolinium Substitution Induced Defect Restructuring in Multiferroic BiFeO<sub>3</sub> Case Study by Positron Annihilation Spectroscopy. *J. Phys. D: Appl. Phys.* 46, 495309 (2013). <https://doi.org/10.1088/0022-3727/46/49/495309>.
  22. A. Mukherjee, S. Basu, G. Chakraborty, and M. Pal, Effect of Y-Doping on the Electrical Transport Properties of Nanocrystalline BiFeO<sub>3</sub>. *J. Appl. Phys.* 112, 014321 (2012). <https://doi.org/10.1063/1.4734005>.
  23. S.J. Chiu, Y.T. Liu, G.P. Yu, H.Y. Lee, and H.J. Huang, The Structure and Ferroelectric Property of La-doped BiFeO<sub>3</sub>/SrTiO<sub>3</sub> Artificial Superlattice Structure by RF Sputtering: Effect of Deposition Temperature. *Thin Solid Films* 529, 85–88 (2013). <https://doi.org/10.1016/j.tsf.2012.02.033>.
  24. M. Zhong, N.P. Kumar, E. Sagar, Z. Jian, H. Yemin, and P.V. Reddy, Structural Magnetic and Dielectric Properties of Y Doped BiFeO<sub>3</sub>. *Mater. Chem. Phys.* 173, 126–131 (2016). <https://doi.org/10.1016/j.matchemphys.2016.01.047>.
  25. M.B. Bellakki and V. Manivannan, Citrate-gel Synthesis and Characterization of Yttrium-Doped Multiferroic BiFeO<sub>3</sub>. *J. Sol-Gel Sci Technol* 53, 184–192 (2010). <https://doi.org/10.1007/s10971-009-2076-1>.
  26. V. Srinivas, A.T. Raghavender, and K. Vijaya Kumar, Structural and Magnetic Properties of Mn Doped BiFeO<sub>3</sub> Nanomaterials. *Phys Resear Int* (2016). <https://doi.org/10.1155/2016/4835328>.
  27. S. Chauhan, M. Kumar, S. Chhoker, S.C. Katyal, H. Singh, M. Jewariya, and K.L. Yadav, Multiferroic, Magnetolectric and Optical Properties of Mn-Doped BiFeO<sub>3</sub> Nanoparticles. *Solid State Commun* 152, 525–529 (2012). <https://doi.org/10.1016/j.ssc.2011.12.037>.
  28. J.Z. Huang, Y. Wang, Y. Lin, M. Li, and C.W. Nan, Effect of Mn Doping on Electric and Magnetic Properties of BiFeO<sub>3</sub> Thin Films by Chemical Solution. *J. Appl. Phys.* 106, 063911 (2009). <https://doi.org/10.1063/1.3225559>.
  29. J. Silva, A. Reyes, R. Castaneda, H. Esparza, H. Camacho, J. Matutes, and L. Fuentes, Structure and Electromagnetic Properties of Bi<sub>1-x</sub>Y<sub>x</sub>Fe<sub>0.95</sub>Mn<sub>0.05</sub>O<sub>3</sub> (x=0.05, 0.075, 0.10). *Ferroelectrics* 426, 103–111 (2012). <https://doi.org/10.1080/00150193.2012.671624>.
  30. R. Palkar, D.C. Kundaliya, and S.K. Malik, Effect of Mn Substitution on Magnetolectric Properties of Bismuth Ferrite System. *J. Appl. Phys.* 93, 4337 (2003). <https://doi.org/10.1063/1.1558992>.
  31. S. Mukherjee, L.A.W. Basu, N.T.K. Green, and M. Thanh, Pal, Enhanced Multiferroic Properties of Y and Mn Codoped Multiferroic BiFeO<sub>3</sub> Nanoparticles. *J. Mater. Sci.* 50, 1891–1900 (2015). <https://doi.org/10.1007/s10853-014-8752-8>.
  32. M. Mukherjee, S. Banerjee, N.T.K. Basu, L.A.W. Thanh, and M. Green, Pal, Enhanced Magnetic and Electrical Properties of Y and Mn co-doped BiFeO<sub>3</sub> Nanoparticles. *Physica B* 448, 199–203 (2014). <https://doi.org/10.1016/j.physb.2014.03.082>.
  33. D. Varshney, A. Kumar, and K. Verma, Effect of A Site and B Site Doping on Structural, Thermal and Dielectric Properties of BiFeO<sub>3</sub> Ceramics. *J. Alloy. Compd.* 509, 8421–8426 (2011). <https://doi.org/10.1016/j.jallcom.2011.05.106>.
  34. K. Momma and F. Izumi, VESTA 3 for Three-Dimensional Visualization of Crystal, Volumetric and Morphology Data. *J. Appl. Crystallogr.* 44, 1272–1276 (2011). <https://doi.org/10.1107/s0021889811038970>.
  35. P. Trivedi, F. Singh, B. Vyas, H. Kundalia, D.K. Shukla, S. Rayaprol, and D.G. Kuberkar, Stiffening of Phonons with Enhanced Hybridization and Structural Phase Transformation Upon Pr-Doping in BiFeO<sub>3</sub>. *Physica B Phys Condens Matt* 571, 247–251 (2019). <https://doi.org/10.1016/j.physb.2019.07.021>.
  36. R.A. Young ed., *The Rietveld Method*. (New York: Oxford University Press), 1993).

37. RA Agarwal, S Sanghi, AN Ahlawat, and Monica, Phase Transformation, Dielectric and Magnetic Properties of Nb-Doped  $\text{Bi}_{0.8}\text{Sr}_{0.2}\text{FeO}_3$  Multiferroics, *J. Appl. Phys.*, 111, 113917 (2012); doi: <https://doi.org/10.1063/1.4728981>
38. F. Huang, Z. Wang, Lu. Xiaomei, J. Zhang, K. Min, W. Lin, R. Ti, Xu. TingTing, Ju. He, C. Yue, and J. Zhu, Peculiar Magnetism of  $\text{BiFeO}_3$  Nanoparticles with Size Approaching the Period of the Spiral Spin Structure. *Sci Rep* 3, 2907 (2013). <https://doi.org/10.1038/srep02907>.
39. D.K. Rana, S.K. Kundu, R.J. Choudhary, and S. Basu, Enhancement of Electrical and Magnetodielectric Properties of  $\text{BiFeO}_3$  Incorporated PVDF Flexible Nanocomposite Films. *Mater Resear Expr* 6, 0850d9 (2019). <https://doi.org/10.1088/2053-1591/ab26de>.
40. A. Khomchenko, I.O. Troyanchuk, D.V. Karpinsky, S. Das, V.S. Amaral, M. Tovar, V. Sikolenko, and J.A. Paixão, Structural Transitions and Unusual Magnetic Behaviour in Mn-doped  $\text{Bi}_{1-x}\text{La}_x\text{FeO}_3$  Perovskites. *J. Appl. Phys.* 112, 084102 (2012). <https://doi.org/10.1063/1.4759435>.
41. R.P. Maiti, S. Basu, and D. Chkaravorty, Synthesis of Nanocrystalline  $\text{YFeO}_3$  and its Magnetic Properties. *J. Magn. Magn. Mater.* 321, 3274–3277 (2009). <https://doi.org/10.1016/j.jmmm.2009.05.061>.
42. B. Deka, S. Ravi, A. Perumal, and D. Pamu, Effect of Mn Doping on Magnetic and Dielectric Properties of  $\text{YFeO}_3$ . *Ceram Int* 43, 1323–1334 (2016). <https://doi.org/10.1016/j.ceramint.2016.10.087>.
43. Wu. Jiangtao, N. Li, Xu. Jun, S. Zhou, Y. Jiang, and Z. Xie, Synthesis, Phase Diagram and Magnetic Properties of  $(1-x)\text{BiFeO}_3-x\text{LaMnO}_3$  Solid Solution. *J. Alloy. Compd.* 634, 142–147 (2015). <https://doi.org/10.1016/j.jallcom.2015.01.283>.
44. A. Wrzesinska, A. Khort, M. Witkowski, J. Szczytko, J. Ryl, J. Gurgul, D.S. Kharitonov, K. Łątka, T. Szumiata, and A. Wypych-Puszkarcz, Structural, Electrical and Magnetic Study of La-, Eu-, and Er-Doped Bismuth Ferrite Nanomaterials Obtained by Solution Combustion Synthesis. *Sci Rep* 11, 22746 (2021). <https://doi.org/10.1038/s41598-021-01983-z>.
45. R. Das, T. Sarkar, and K. Mandal, Multiferroic Properties of  $\text{Ba}^{2+}$  and  $\text{Gd}^{3+}$  Co-Doped Bismuth Ferrite: Magnetic, Ferroelectric and Impedance Spectroscopic Analysis. *J. Phys. D: Appl. Phys.* 45, 455002 (2012). <https://doi.org/10.1088/0022-3727/45/45/455002>.
46. S.K. Pradhan and B.K. Roul, Effect of Gd Doping on Structural, Electrical and Magnetic Properties of  $\text{BiFeO}_3$  Electroceramic. *J. Phys. Chem. Solids* 72, 1180–1187 (2011). <https://doi.org/10.1016/j.jpcs.2011.07.017>.

**Publisher's Note** Springer Nature remains neutral with regard to jurisdictional claims in published maps and institutional affiliations.